


Article

Essential Electronic Properties of Stage-1 Li/Li⁺-Graphite-Intercalation Compounds for Different Concentrations

Wei-Bang Li ^{1,*}, Shih-Yang Lin ², Ming-Fa Lin ^{1,3} and Kuang-I Lin ^{4,*}¹ Department of Physics, National Cheng Kung University, Tainan 701, Taiwan; mflin@mail.ncku.edu.tw² Department of Physics, National Chung Cheng University, Chiayi 621, Taiwan; sylin.1985@gmail.com³ Hierarchical Green-Energy Materials (Hi-GEM) Research Center, National Cheng Kung University, Tainan 701, Taiwan⁴ Core Facility Center, National Cheng Kung University, Tainan 701, Taiwan

* Correspondence: weibang1108@gmail.com (W.-B.L.); kilin@mail.ncku.edu.tw (K.-I.L.)

Abstract: We use first-principles calculations within the density functional theory (DFT) to explore the electronic properties of stage-1 Li- and Li⁺-graphite-intercalation compounds (GIC) for different concentrations of LiC_x/Li⁺C_x, with x = 6, 12, 18, 24, 32 and 36. The essential properties, e.g., geometric structures, band structures and spatial charge distributions are determined by the hybridization of the orbitals, the main focus of our work. The band structures/density of states/spatial charge distributions display that Li-GIC shows a blue shift of Fermi energy just like metals, but Li⁺-GIC still remains as in the original graphite or exhibits so-called semi-metallic properties, possessing the same densities of free electrons and holes. According to these properties, we find that there exist weak but significant van der Waals interactions between interlayers of graphite, and 2s-2p_z hybridization between Li and C. There scarcely exist strong interactions between Li⁺-C. The dominant interaction between the Li and C is 2s-2p_z orbital-orbital coupling; the orbital-orbital coupling is not significant in the Li⁺ and C cases, but dipole-dipole coupling is.

Keywords: first-principles; graphite intercalation compounds

Citation: Li, W.-B.; Lin, S.-Y.; Lin, M.-F.; Lin, K.-I. Essential Electronic Properties of Stage-1 Li/Li⁺-Graphite-Intercalation Compounds for Different Concentrations. *Condens. Matter* **2022**, *7*, 35. <https://doi.org/10.3390/condmat7020035>

Academic Editors: Mohsen Asle Zaeem, Siby Thomas and K.M. Ajith

Received: 29 March 2022

Accepted: 26 April 2022

Published: 5 May 2022

Publisher's Note: MDPI stays neutral with regard to jurisdictional claims in published maps and institutional affiliations.



Copyright: © 2022 by the authors. Licensee MDPI, Basel, Switzerland. This article is an open access article distributed under the terms and conditions of the Creative Commons Attribution (CC BY) license (<https://creativecommons.org/licenses/by/4.0/>).

1. Introduction

Green energy is one of the most important issues in the world today. The limited resources, such as fossil fuels, will be consumed eventually. In addition, the concomitant environmental pollution is also inevitable. This therefore gives rise to the need for efficient storage of electrical energy. Apart from the finite resources on earth, solar power has the most potential for humans. As years passed, rechargeable batteries have emerged as a solution to the energy storage problem. Many previous theoretical and experimental studies focused on lithium batteries and lithium-ion batteries because of the low costs, high safety and long cycle life. For the most part, the anodes are composed of carbon and non-carbon materials. The former is the well-known graphite, and the latter can be lithium, sodium or other ionic clusters. This kind of anode is almost always presented as graphite-intercalation compounds (GICs), that is to say, the lithium atoms (or other atoms) are intercalated into the graphite layers.

Graphite with its layered structure is easily intercalated by alkali-metal atoms. The carbon-layered system is purely composed of a hexagonal symmetric lattice, in which there exist weak but significant van der Waals (vdW) interactions. The vdW interactions modify the low-lying energy band structures and dominate the essential physical properties of the graphite of GIC. The electronic properties strongly depend on the stacking configurations the graphitic layers. In general, there are three well known kinds of stacking configurations: AA (simple hexagonal), AB (Bernal), and ABC (rhombohedral) [1–3]. Previous studies [4] revealed that the Li-GICs and A-GICs (A stands for an alkali metal such as Na, K, Rb, or Cs)

present different structures in stage-1: LiC_6 and AC_8 , respectively. Additionally, the AA-stacking configuration is the most stable one for Li-GIC of stage-1 type [5], whereas other stage- n types ($n = 2,3,4 \dots$) form the AB-stacking configuration. The comparisons between Li-GICs and A-GICs have been widely discussed in the past years, but few theoretical and experimental research papers on Li-ion-GICs and alkali-ion-GICs are available. The geometric properties of Li-GICs, such as disorder on surface [6] or interlayer distances [7], have been studied for years. However, many studies exclusively focused on Li-atom intercalation/deintercalation, but ignored Li-ion cases.

In this work, we display the comparison between Li-GICs and Li^+ -GICs, and mainly focus on the orbital hybridizations in lithium and lithium-ion GICs by presenting the essential structural and electronic properties. We consider the different concentrations on the uniform situations of intercalations, i.e., this paper only covers the stage-1 type for different concentrations. In addition, the optimal adatom position is located in the hollow site [8–11] of the hexagonal carbon layers. The theoretical calculations, including the tight-binding model and DFT method [12–15], are utilized to investigate the total ground state energies, optimal geometric structures, energy band structures, density of states and the spatial charge distributions. For instance, the DFT method is used to examine the band structures and interlayer binding, finding that for any number of layers, Bernal few-layer graphenes (AB stacking) are the most stable [12]. Furthermore, the band structures predicted by DFT on ABA-stacked and ABC-stacked trilayer graphenes are fitted to a tight-binding model [13,15]. Moreover, the intercalation-induced conduction-electron densities can be predicted. The rich and unique phenomena in Li-GICs and Li^+ -GICs are expected to show significant differences under a systematic comparison with each other.

2. Theoretical Calculations

The density functional theory (DFT) [16–19] has been widely utilized for the many-electron systems in physics and chemistry for years. Specifically, the Vienna ab initio simulation package (VASP) [20] evaluates an approximate solution within the density functional theory by solving the Kohn-Sham equations. We used first-principle calculations with the VASP in this study. The VASP applies Bloch's theorem because it is suitable for dealing with the problems of bulk materials with periodic boundary conditions. The exchange-correlation energy depending on the electron-electron interactions was calculated from the Perdew-Burke-Ernzerhof functional under a generalized gradient approximation (GGA) [21]. First, all the atoms in the relaxation process were adjusted to form the optimized structures with the lowest total ground energy. The spatial charge density can be solved by a numerically self-consistent scheme. Furthermore, we can use the above results to investigate the fundamental physical properties. The first Brillouin zone was sampled in a Gamma scheme by a $10 \times 10 \times 10$ k-point mesh for optimization and a $30 \times 30 \times 30$ k-point mesh for electronic structures. The energy convergence was set to 10^{-5} eV for two simulation steps. The maximum Hellmann-Feynman force on each atom was less than $0.01 \text{ eV}/\text{\AA}$. The calculations for Li^+ ion in this work were performed by reducing the number of electrons by fixing the NELECT tag in the INCAR file, and the Vander Waals interactions were considered with the tag IVDW = 11, which is under the DFT-D3 method of Grimme.

3. Results and Discussions

3.1. Geometric Structures

The geometric symmetries of graphite are diversified by the chemical intercalation. The Li/Li^+ can be easily intercalated into the interlayer spacing because of the weak but significant van der Waals interactions. There are three frequent types of absorptions positions, the hollow sites, the top sites, and the bridge sites, for the intercalant atoms. The hollow-site position possesses the lowest ground energies, that is to say, the hollow-site position is the most stable geometric configuration [22,23]. The pristine structures of $\text{LiC}_x/\text{Li}^+\text{C}_x$ display the same stacking type, stage-1, but distinct concentrations, listed in

Table 1. The changes between the interlayer distances of Li-GIC/Li⁺-GIC are very different from each other.

Table 1. Optimized interlayer distances for state-1 AA-stacking graphite and Li/Li⁺ GICs with PBE functional methods.

	Interlayer Distance (Å)
LiC ₆	3.815
LiC ₁₂	3.863
LiC ₁₈	3.924
LiC ₂₄	3.954
LiC ₃₂	3.978
LiC ₃₆	3.964
Li ⁺ C ₆	3.082
Li ⁺ C ₁₂	3.283
Li ⁺ C ₁₈	3.374
Li ⁺ C ₂₄	3.451
Li ⁺ C ₃₂	3.510
Li ⁺ C ₃₆	3.555
Graphite	3.550

For the atom cases, the interlayer distances of LiC₆, LiC₁₂, LiC₁₈, LiC₂₄, LiC₃₂ and LiC₃₆ are 3.815 Å, 3.863 Å, 3.924 Å, 3.954 Å, 3.987 Å and 3.964 Å, respectively; for the ion cases, the interlayer distances of Li⁺C₆, Li⁺C₁₂, Li⁺C₁₈, Li⁺C₂₄, Li⁺C₃₂ and Li⁺C₃₆ are 3.082 Å, 3.283 Å, 3.374 Å, 3.451 Å, 3.510 Å and 3.555 Å, respectively. See Table 1 for details.

The heights of LiC_x and Li⁺C_x decrease with higher concentrations. Apparently, compared to the pristine graphite lattice with an experimental interlayer distance of 3.550 Å [1], the height of the former will be close to that of pristine graphite when the concentration rises; on the contrary, the height of the latter will be close to that of the pristine graphite lattice when the concentration declines (Figure 1).

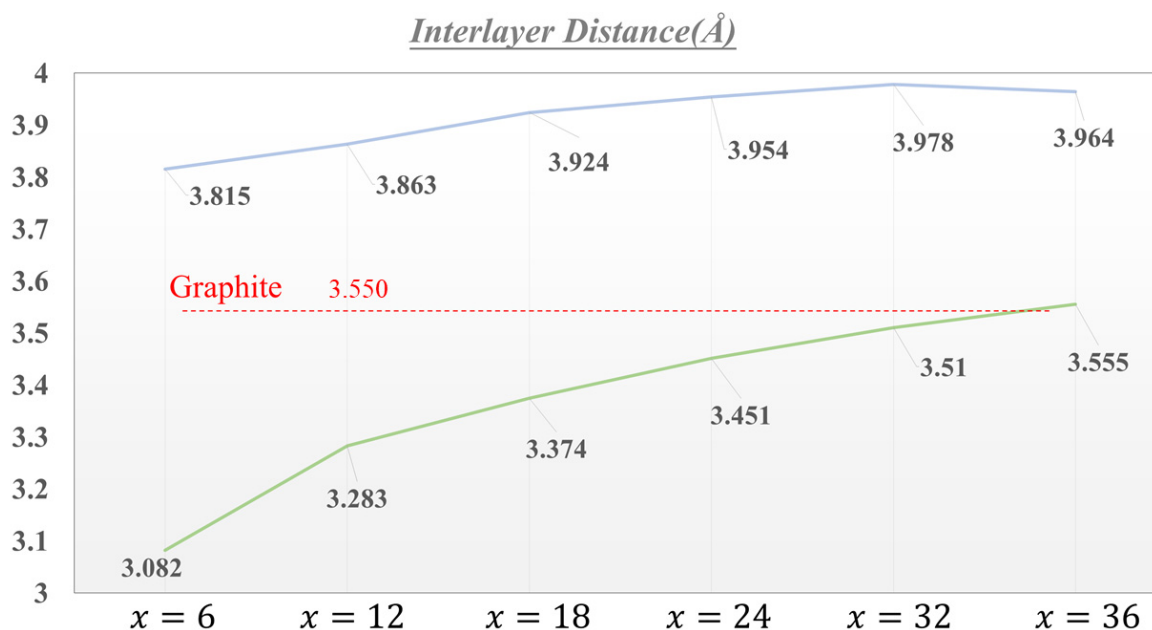


Figure 1. The interlayer distances with different concentrations. The blue, green, and red lines are the interlayer distances of Li-GICs, Li⁺-GICs, and AA-stacking graphite.

3.2. Band Structures and Density of States

The pristine AA-stacking graphite possesses an unusual electronic structure, including the same amounts of free electrons and holes within -0.5 eV \sim 0.5 eV, according to the band structure and density of state (Figure 2), and an obvious band overlap is revealed in the kz -dependent energy dispersion along ΓA . That is to say, the AA-stacking graphite behaves like a semimetal. The low-lying energy bands (π bands) are dominated by the C- $2p_z$ orbitals; the C-($2s$, $2p_x$, $2p_y$) orbitals, generating the σ bands, appear at $E \leq -3.0$ eV and strongly contribute to form the planar geometric structures. However, the electronic band structures exhibit very different changes after the intercalation of Li and Li^+ .

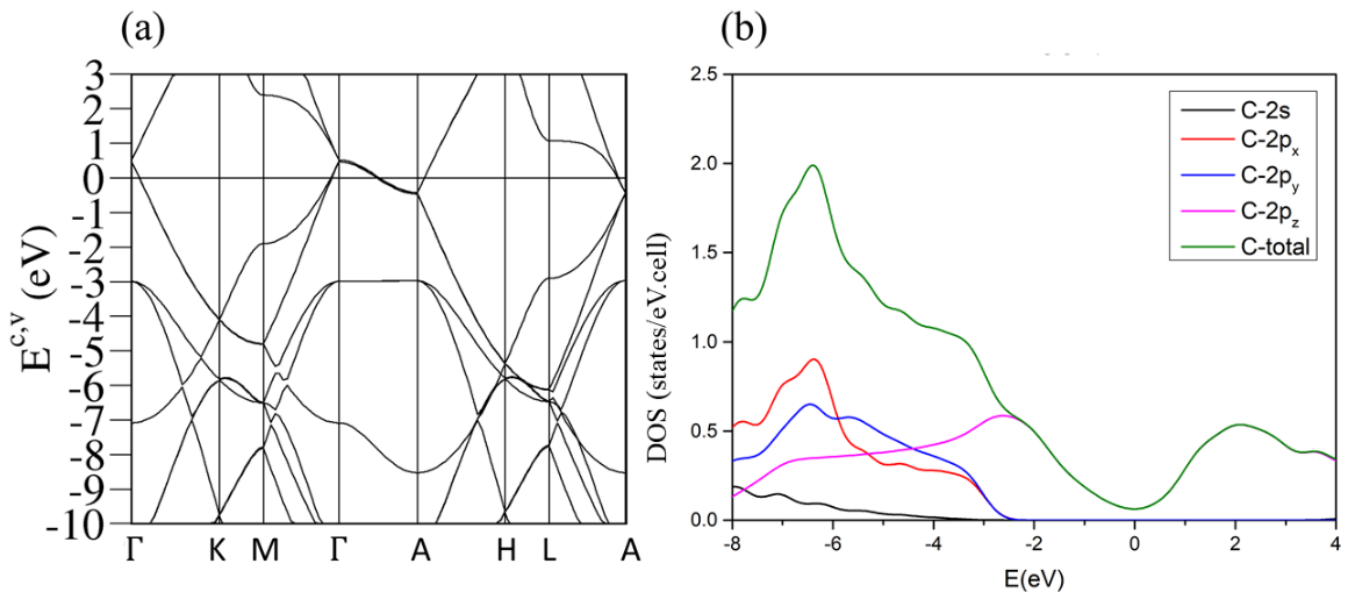


Figure 2. The (a) band structure and (b) density of state of AA-stacking graphite.

For intercalations of Li atoms, the asymmetry of the electron and hole bands becomes much more noticeable. Apparently, the Fermi level presents a blue shift, compared to the pristine graphite, and does not intersect with any valence bands (Figure 3). That is to say, the free conduction electrons are all created by the intercalations of Li atoms and replace the pristine carriers (both electron and hole). The blue shift of the Fermi level is determined by the negative energy with the minimum density of state and the E_F ($E = 0$); the values are calculated to be, respectively, 1.800 eV, 1.326 eV, 1.138 eV, 0.991 eV, 0.882 eV and 0.810 eV for $x = 6, 12, 18, 24, 32$ and 36 , as shown in Figure 4. These results indicate that the C- $2p_z$ orbitals are easily affected by the Li-C bonds and sensitive to the concentrations of Li-atom intercalation.

The intercalations of Li^+ ions are quite different from the Li case. The band structures do not exhibit the apparent shift of the Fermi level, estimated to be 0.088 eV, 0.042 eV, 0.036 eV, 0.026 eV, 0.018 eV and 0.026 eV for $x = 6, 12, 18, 24, 32$ and 36 , respectively, as shown in Figure 4; that is, the Fermi level maintains a position similar to the pristine graphite. Moreover, the initial σ bands display shoulder structures in the orbital-projected density of states near -2.6 eV \sim -2.9 eV at the Γ point, and present a blue shift relatively to the Li ones; in other words, the σ bands are deeper or more stable in the Li intercalations than in the Li^+ ones.

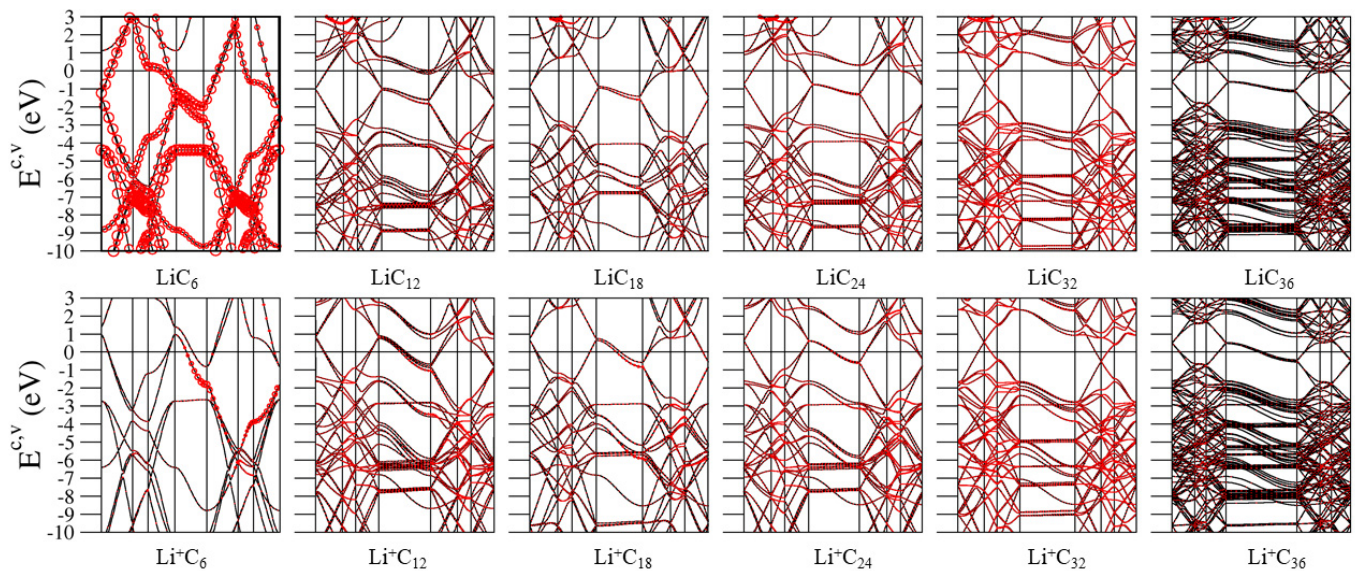


Figure 3. The band structures for Li-GICs and Li⁺-GICs.

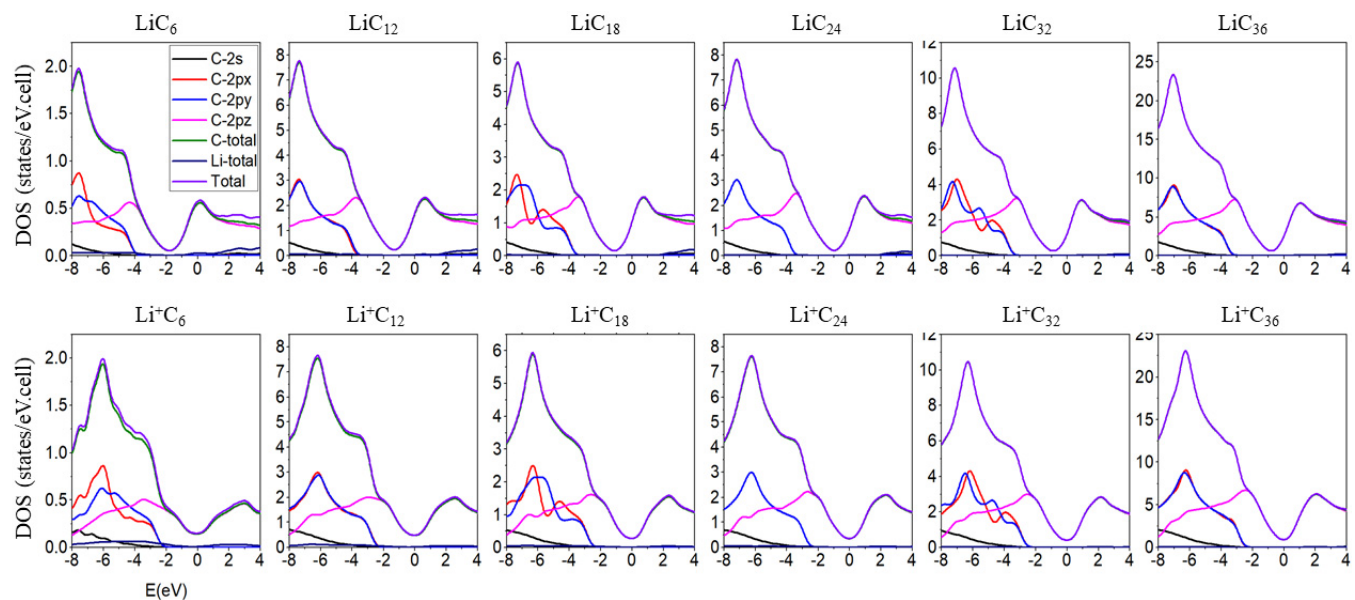


Figure 4. The density of states and the shifts of the lowest values to Fermi level for Li-GICs and Li⁺-GICs.

3.3. Charge Distributions and Charge Transfer

The spatial charge distributions (ρ) and variations ($\Delta\rho$) of Li- and Li⁺-GICs are illustrated in Figures 4 and 5. The ρ is directly obtained from the calculated charge density, but the $\Delta\rho$ is a value subtracting the charge density of the pure Li (or Li⁺) and of the pure C charge density from the charge density of the Li-GIC (or Li⁺-GIC). They are all shown on a x - z plane and useful for understanding the chemical bonding change after intercalations. For Li-atom intercalations, the ρ and $\Delta\rho$ indicate that significant hybridizations of Li-C bonds with red and yellow colors in Figure 6 (within the red dashed frame) depend on the concentration; the variations become obvious with an increase of concentrations, i.e., the charge transfer is strongest in LiC₆, but weakest in LiC₃₆. Moreover, the variations are close to the C atoms but not the Li atoms, indicating that the charge transfer took place from the Li atom to the C atom. Additionally, the charge transfer mainly appears on the C atoms directly neighboring Li atoms.

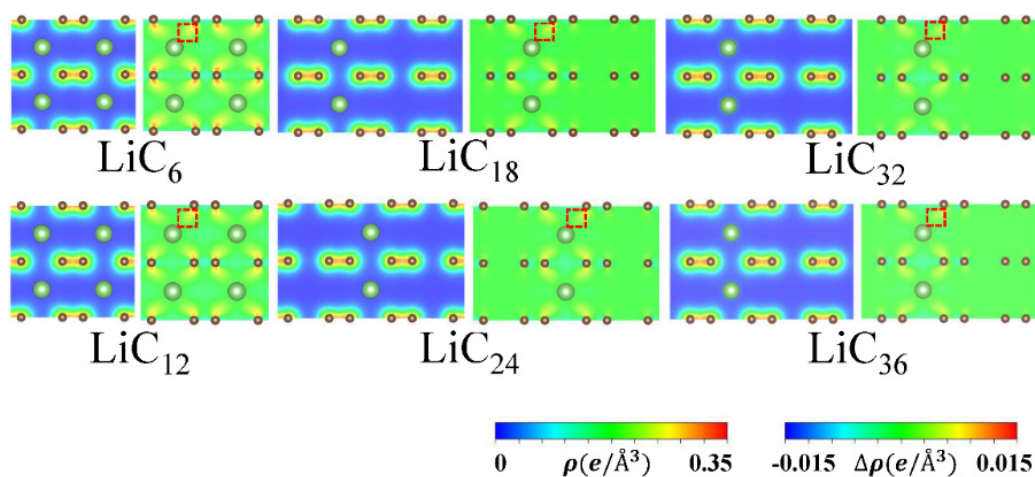


Figure 5. The spatial charge distributions and variations of Li-GICs.

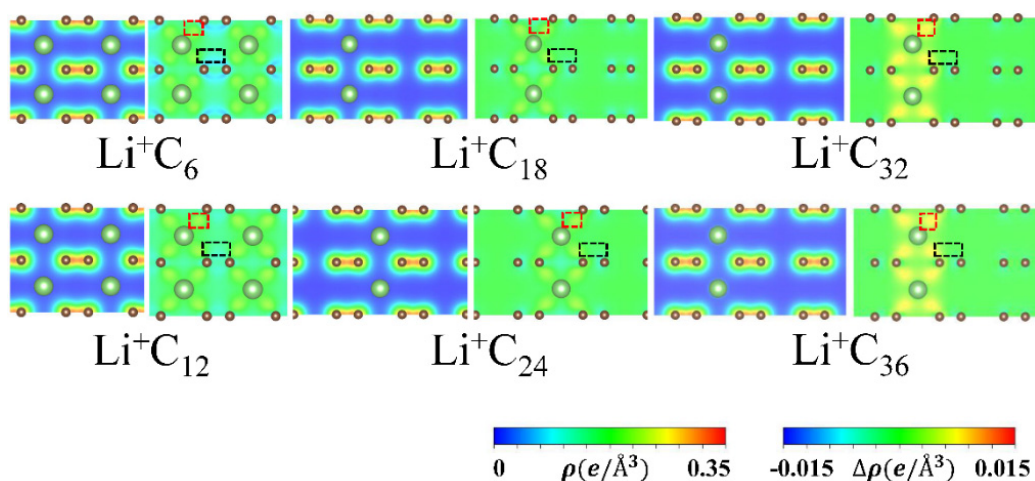


Figure 6. The spatial charge distributions and variations of Li⁺-GICs.

For Li⁺-ion intercalations, the variations present quite different characteristics. The $\Delta\rho$ between the Li⁺ ions and the C atoms are broader and lighter than for the Li-atom cases, shown with light green and yellow colors in Figure 6 (within the red dash frame). In addition, the $\Delta\rho$ between the neighboring C atoms become more obvious with an increase of concentrations, as seen by the light blue colors in Figure 6 (within the black dash frame); moreover, the variations between the Li⁺ ions and the C atoms are slightly closer to the former. That is to say, the charge transfer occurs from the C atoms to the Li⁺ ions. This is similar to the Li-atom case in the sense that the carbon atoms not directly neighboring the Li⁺ ions are seldom affected. By the Bader analysis in the VASP calculations, the Li-GICs exhibit charge transfers for LiC₆, LiC₁₂, LiC₁₈, LiC₂₄, LiC₃₂ and LiC₃₆, respectively; the Li⁺-GICs exhibit charge transfers for Li⁺C₆, Li⁺C₁₂, Li⁺C₁₈, Li⁺C₂₄, Li⁺C₃₂ and Li⁺C₃₆, respectively, as shown in Table 2. The charge transfers show apparent differences between the Li-GIC and the Li⁺-GIC. For the former, the charge transfers from the Li atoms to the C atoms so that the charges per Li atom exhibit a minus value. Moreover, there are slightly differences in charge transfers of the Li atoms with different concentrations. However, the C atoms obtain charges from the Li atoms, where the values of charge transfers of C atoms increase with the concentration. In other words, the higher the concentrations are, the stronger is the C-Li bonding. On the contrary, in the Li⁺ cases, the Li⁺ ion attracts charges from the C atoms. Even though the calculated values show that the charge transfers are much more in the Li⁺C₆ than in the Li⁺C₃₆, the charge transfers of the C atoms are still less than 0.3 charges, which result in the relatively weak interactions.

Table 2. The charge transfers of Li-GICs and Li⁺-GICs.

	Charge Transfer (e/atom)	
	C	Li
LiC ₆	0.144	−0.865
LiC ₁₂	0.073	−0.871
LiC ₁₈	0.049	−0.878
LiC ₂₄	0.037	−0.880
LiC ₃₂	0.028	−0.884
LiC ₃₆	0.025	−0.883
Li ⁺ C ₆	−0.030	0.191
Li ⁺ C ₁₂	−0.015	0.176
Li ⁺ C ₁₈	−0.009	0.173
Li ⁺ C ₂₄	−0.007	0.163
Li ⁺ C ₃₂	−0.005	0.159
Li ⁺ C ₃₆	−0.004	0.155

4. Conclusions

In summary, we present the current work from first-principles calculations within the GGA method. Our work provides a comparison between these two cases and gives the evidence for the orbital hybridizations. We find that the changes of essential physical properties are very different between Li- and Li⁺-GICs, e.g., the interlayer distances, energy band structures, density of states and the spatial charge distributions, and the results clearly reveal that the Li-C bonds are generated from the 2s-2p_z orbital hybridizations, which leads to the high charge transfers from Li to C of about 0.86–0.88 electrons as well. On the contrary, the variations of Li⁺-GICs are relatively weak, and the charge transfers that Li⁺ obtains from C merely range from 0.163–0.191 electrons. The dominant effects between Li and C are obviously the orbital-orbital interactions; but between Li⁺ and C, the main effects might be the dipole-dipole interactions. The saturated electronic configurations of the Li⁺ ions, similar to the inert gas helium [He], lead to a low contribution of free electron carriers.

Author Contributions: Data curation, M.-F.L.; Methodology, S.-Y.L.; Writing—original draft, W.-B.L.; Writing—review & editing, K.-I.L. All authors have read and agreed to the published version of the manuscript”.

Funding: This work is supported by the Hi-GEM Research Center and the Taiwan Ministry of Science and Technology under grant numbers MOST 108-2212-M-006-022-MY3, MOST 108-3017-F-006-003 and MOST 109-2811-M-006-505.

Institutional Review Board Statement: Not applicable.

Informed Consent Statement: Not applicable.

Data Availability Statement: Not applicable.

Conflicts of Interest: The authors declare no conflict of interest.

References

1. Lee, J.K.; Lee, S.C.; Ahn, J.P.; Kim, S.C.; Wilson, J.I.; John, P. The growth of AA graphite on (111) diamond. *J. Chem. Phys.* **2008**, *129*, 234709. [[CrossRef](#)] [[PubMed](#)]
2. Yankowitz, M.; Wang, J.I.J.; Birdwell, A.G.; Chen, Y.A.; Watanabe, K.; Taniguchi, T.; Jacquod, P.; San-Jose, P.; Jarillo-Herrero, P.; LeRoy, B.J. Electric field control of soliton motion and stacking in trilayer graphene. *Nat. Mater.* **2014**, *13*, 786789. [[CrossRef](#)] [[PubMed](#)]

3. Coletti, C.; Forti, S.; Principi, A.; Emtsev, K.V.; Zakharov, A.A.; Daniels, K.M.; Daas, B.K.; Chandrashekar, M.V.S.; Ouisse, T.; Chaussende, D.; et al. Revealing the electronic band structure of trilayer graphene on SiC: An angle-resolved photoemission study. *Phys. Rev. B* **2013**, *88*, 155439. [[CrossRef](#)]
4. Kaneko, T.; Saito, R. First-principles study on interlayer state in alkali and alkaline earth metal atoms intercalated bilayer graphene. *Surf. Sci.* **2017**, *665*, 1–9. [[CrossRef](#)]
5. Rydberg, H. Van der Waals Density Functional for Layered Structures. *Phys. Rev. Lett.* **2003**, *91*, 126402. [[CrossRef](#)] [[PubMed](#)]
6. Sethuraman, V.A.; Hardwick, L.J.; Srinivasan, V.; Kostecky, R. Surface structural disordering in graphite upon lithium intercalation/deintercalation. *J. Power Sources* **2010**, *195*, 3655–3660. [[CrossRef](#)]
7. Park, T.R.; Rhee, S.S. Multilayer model of interlayer spacing in graphite intercalation compounds. *Appl. Phys. A* **2001**, *72*, 367–372. [[CrossRef](#)]
8. Chan, K.T.; Neaton, J.B.; Cohen, M.L. First-principles study of metal adatom adsorption on graphene. *Phys. Rev. B* **2008**, *77*, 235430. [[CrossRef](#)]
9. Jin, K.H.; Choi, S.M.; Jhi, S.H. Crossover in the adsorption properties of alkali metals on graphene. *Phys. Rev. B* **2010**, *82*, 033414. [[CrossRef](#)]
10. Praveen, C.S.; Piccinin, S.; Fabris, S. Adsorption of alkali adatoms on graphene supported by the Au/Ni (111) surface. *Phys. Rev. B* **2015**, *92*, 075403. [[CrossRef](#)]
11. Lin, S.Y.; Lin, Y.T.; Tran, N.T.T.; Su, W.P.; Lin, M.F. Feature-rich electronic properties of aluminum-doped graphenes. *arXiv* **2016**, arXiv:1606.01624.
12. Aoki, M.; Amawashi, H. Dependence of band structures on stacking and field in layered graphene. *Solid State Commun.* **2007**, *142*, 123–127. [[CrossRef](#)]
13. Zhang, F.; Sahu, B.; Min, H.; MacDonald, A.H. Band structure of A B C-stacked graphene trilayers. *Phys. Rev. B* **2010**, *82*, 035409. [[CrossRef](#)]
14. Avramov, P.V.; Sakai, S.; Entani, S.; Matsumoto, Y.; Naramoto, H. Ab initio LC-DFT study of graphene, multilayer graphenes and graphite. *Chem. Phys. Lett.* **2011**, *508*, 86–89.
15. Menezes, M.G.; Capaz, R.B.; Louie, S.G. Ab initio quasiparticle band structure of ABA and ABC-stacked graphene trilayers. *Phys. Rev. B* **2014**, *89*, 035431. [[CrossRef](#)]
16. Persson, K.; Hinuma, Y.; Meng, Y.S.; Van der Ven, A.; Ceder, G. Thermodynamic and kinetic properties of the Li-graphite system from first-principles calculations. *Phys. Rev. B* **2010**, *82*, 125416. [[CrossRef](#)]
17. Wang, Z.; Selbach, S.M.; Grande, T. Van der Waals density functional study of the energetics of alkali metal intercalation in graphite. *RSC Adv.* **2014**, *4*, 4069. [[CrossRef](#)]
18. Lin, S.Y.; Chang, S.L.; Tran, N.T.T.; Yang, P.H.; Lin, M.F. H-Si bonding-induced unusual electronic properties of silicene: A method to identify hydrogen concentration. *Phys. Chem. Chem. Phys.* **2015**, *39*, 26443–26450. [[CrossRef](#)]
19. Rafique, M.; Unar, M.A.; Ahmed, I.; Chachar, A.R.; Shuai, Y. Ab-initio investigations on physisorption of alkaline earth metal atoms on monolayer hexagonal boron nitride (h-BN). *J. Phys. Chem. Solids* **2018**, *118*, 114–125. [[CrossRef](#)]
20. Perdew, J.P.; Burke, K.; Ernzerhof, M. Generalized gradient approximation made simple. *Phys. Rev. Lett.* **1996**, *77*, 3865. [[CrossRef](#)]
21. Blchl, P.E. Projector augmented-wave method. *Phys. Rev. B* **1994**, *50*, 17953. [[CrossRef](#)] [[PubMed](#)]
22. Dresselhaus, M.S.; Dresselhaus, G. Intercalation compounds of graphite. *Adv. Phys.* **2002**, *51*, 1–186. [[CrossRef](#)]
23. Okamoto, Y. Density functional theory calculations of alkali metal (Li, Na, and K) graphite intercalation compounds. *J. Phys. Chem. C* **2013**, *118*, 16–19. [[CrossRef](#)]